文章编号：1001-9014(2025)03-0394-12

DOI:10. 11972/j. issn. 1001-9014. 2025. 03. 009

Study on correlation of thermal model to in-orbit data for infrared optical payloads on FY-3E/HIRAS-II

LI Yu-Han[1,2], YANG Bao-Yu[1,2*], ZHANG Qiang[1], GUO Zhi-Peng[1], WU Yi-Nong[1,2], TANG Xiao[1,2], LI Shang-Ju[1,2]

(1. Shanghai Institute of Technical Physics, Chinese Academy of Sciences, Shanghai 200083, China;
2. University of Chinese Academy of Sciences, Beijing 100049, China)

Abstract: The Infrared Hyperspectral Atmospheric Sounder II (HIRAS-II) is the key equipment on FengYun-3E (FY-3E) satellite, which can realize vertical atmospheric detection, featuring hyper spectral, high sensitivity and high precision. To ensure its accuracy of detection, it is necessary to correlate their thermal models to in-orbit data. In this work, an investigation of intelligent correlation method named Intelligent Correlation Platform for Thermal Model (ICP-TM) was established, the advanced Kriging surrogate model and efficient adaptive region optimization algorithm were introduced. After the correlation with this method for FY-3E/HIRAS-II, the results indicate that compared with the data in orbit, the error of the thermal model has decreased from 5 K to within ±1 K in cold case (10 ℃). Then, the correlated model is validated in hot case (20 ℃), and the correlated model exhibits good universality. This correlation precision is also much superiors to the general ones like 3 K in other similar literature. Furthermore, the process is finished in 8 days using ICP-TM, the efficiency is much better than 3 months based on manual. The results show that the proposed approach significantly enhances the accuracy and efficiency of thermal model, this contributes to the precise thermal control of subsequent infrared optical payloads.

Key words: thermal model, intelligent correlation method, surrogate model, infrared optical payload, FY-3E

基于在轨数据的FY-3E/HIRAS-II红外光学载荷热模型标校研究

李玉涵[1,2], 杨宝玉[1,2*], 张 强[1], 郭志鹏[1], 吴亦农[1,2], 唐 晓[1,2], 李尚举[1,2]

(1. 中国科学院上海技术物理研究所,上海 200083;
2. 中国科学院大学,北京 100049)

摘要:红外高光谱大气探测仪II(HIRAS-II)是风云三号E星(FY-3E)上的关键设备,具有高光谱、高灵敏度和高精度的垂直大气探测能力。为了确保探测精度,需要将其热模型与在轨温度数据进行标校。本研究中,通过引入先进的克里金代理模型和高效的自适应区域优化算法,建立了一种智能化、自动化、精准化的标校方法,命名为智能热模型标校平台(ICP-TM)。利用该方法对FY-3E/HIRAS进行热模型标校后,结果表明,与在轨数据相比,热模型的预测误差在低温工况(10 ℃)下从5 K降低到±1 K以内。随后在高温工况(20 ℃)下验证了标校后的模型,该模型在不同工况下表现出良好的通用性。这种标校精度也优于其他类似文献中的误差值(如3 K)。此外,使用ICP-TM平台完成该标校过程仅用了8天,效率远高于基于手动标校方法的3个月时间成本。这说明所提出的方法显著提高了热模型的精度和效率,有助于后续红外光学载荷的在轨精密热控研究。

关 键 词:热模型;智能标校方法;代理模型;红外光学载荷;风云三号05星

中图分类号:V11　　**文献标识码**:A

Received date: 2024-08-17, **revised date**: 2024-10-17　　**收稿日期**:2024-08-17,**修回日期**:2024-10-17

Foundation item: Supported by the National Key Research and Development Program of China(2022YFB3904803)

Biography: LI Yu-Han (1997-), female, Jinan, Ph. D. candidate. Research area involves thermal design of optics in space and correlation of thermal models. E-mail: liyuhan202@mails. ucas. ac. cn.

* **Corresponding author**: E-mail: byyang@mail. sitp. ac. cn

Introduction

The FY-3 meteorological satellite, as China's second-generation polar-orbiting meteorological satellite, plays a vital role in disaster prevention and mitigation, as well as in responding to climate change. Building on the success of the FY-3 meteorological satellite, there are higher demands on the consistency of the thermal management for the latest advanced space infrared radiometric benchmark payload technology and the next-generation FY meteorological satellite's quantitative remote sensing infrared payload technology.

The infrared optical payloads on satellites have extremely stringent requirements for the thermal environment. On one hand, thermal deformation can lead to a decline in the imaging quality of the optical system, thus affecting overall imaging performance. On the other hand, thermal noise reduces the detection sensitivity of the optical system, impacting its detection capabilities. Consequently, it is urgent to solve the challenge of accurately correlating thermal models. A precise thermal model is obtained by correcting the parameters of thermal design model, like radiation properties, thermal coupling parameters, and material thermal properties using experimental data or in-orbit data. And finally, obtain a thermal model that can more accurately predict the in-orbit temperature conditions.

Actually, the thermal model correlation problem is an inversion problem of model parameters. There are two main approaches for addressing such inversion problems: deterministic method and statistical method. ① Deterministic method. It treats both the model parameters and the measured temperature data as fixed, known variables. These methods construct a thermal equilibrium equation and solve for the thermal network model parameters using algebraic techniques, yielding a solution with deterministic significance. ② Statistical method. It treats both the model parameters and the measured temperature data as random variables. This method applies statistical techniques to determine the probability distribution of the model temperatures, with the resulting parameters being statistical estimates.

Initially, scholars primarily employed deterministic method to address the problem of thermal model correction. Notable studies in this area includes Toussaint[1] proposed the use of minimizing analysis of experimental energy balance residuals for model correlation. Ishimoto et al. [2] applied linear regression analysis to approximately estimate the radiation heat transfer coefficient and incorporated noise disturbance estimation through Kalman filtering. Shimoji[3] introduced a statistical approach, using statistical regression to modify the thermal network model. By analyzing experimental data and utilizing the F-test (variance test) to determine confidence intervals for critical nodes, this method allowed for the modification of the thermal networks heat transfer coefficient with minimal experimental data, thereby integrating statistical methods into model correlation.

With the increasing complexity of satellite structures, the number of nodes in thermal analysis models can easily reach hundreds of thousands or even millions, significantly increasing the number of parameters requiring correction. At this scale, traditional deterministic method became inadequate for handling the correlation process, Boisvert and statistical methods have gained prominence. Harvey et al. [4] introduced a stochastic approximation method for satellite antenna design, focusing on the selection and optimization of design parameters such as the antenna's orientation relative to Earth and the Sun, as well as environmental parameters. Later, Herrera and Sepulveda [5] were the first to propose applying the Monte Carlo stochastic approximation method to satellite thermal analysis. Since then, the Monte Carlo method and its variants have become mainstream in thermal model correlation and remain highly relevant, forming the foundation for numerous improved techniques.

Both approaches offer distinct ways to infer model parameters based on available data, with deterministic methods providing exact solutions and statistical methods offering probabilistic insights. In recent years, some new methods have emerged. The summary and comparison are shown in Table 1.

It can be observed that when the number of pending parameters in the model decreases, it becomes easier to achieve higher correction accuracy. Although some liter-

Table 1 Summary of the relevant research
表 1 相关研究总结

Researchers	Method	Effect	Project	Number of parameters
Beck et al. [6]	APSO (Adaptive Particle Swarm Optimization)	Error from 4.2 °C±3.2 °C	Bepi Colombo laser altimeter (BELA) receiver baffle structural	10
Anglada et al. [7-8]	Gradient-based methods	Error from 8.71 °C to below 0.31 °C	International space station	6
Kim et al. [9]	Pure thermal methods for modifying thermal resistance, surface properties, and thermal loads	Error more than 80 % of components below 3K	A 6U nanosatellite of SNIPE (Small scale magNetospheric and Ionospheric Plasma Experiment) mission	20
Shin et al. [10]	Surrogate modeling of DNN (Deep Neural Network) and RBF (Radial Basis Function)	Error within 5 K	A typical spacecraft	95
Li et al. [11]	Kriging surrogate model	Error from 4.07 K to 1.22 K by 70.0%	A battery pack	5
Cui et al. [12]	Kriging surrogate model	Error from 3.55 K to 1.11 K	A solar spectrometer	15

ature may have achieved high precision, their models are often too simplistic to be directly applied to practical projects. For the entire model, typically consisting of at least a dozen parameters, the current accuracy can only reach around 3 [9]~5 K[10], which can not meet our requirements of the infrared payloads on the next-generation FY meteorological satellite obviously.

Based on these requirements, an intelligent correlation platform has been developed for the correlation of thermal models to in-orbit data for infrared optical payloads for the first time. The so-called Intelligent Correlation Platform for Thermal Model (ICP-TM), which employs advanced surrogate models, efficient sensitivity analysis, and novel optimization algorithms, achieves a highly accurate thermal model. The enhancement in prediction accuracy and efficiency achieved by this method will be validated through case studies of FY-3E/HIRAS-II under various operating conditions.

1 Thermal case of FY-3E/HIRAS-II

1.1 Background

FY-3E[13] is in a dawn-dusk orbit with an altitude of 836 km, an eccentricity of 0 and an inclination angle of 98.753°. The flight direction is shown in Figure 1(a), where $+Z$ direction is towards the ground, and $+X$ direction is the flight direction. The structure of each component is shown in Figure 1(a) and Figure 1(b). The main body of the enclosure measures 750 mm×650 mm×300 mm. The main temperature control targets are the interferometer and the baseplate. The former is the primary temperature-controlled payload, while the latter represents the overall temperature level of the optical instrument. These two temperatures are regulated by PID (Proportional Integral Derivative) controllers, monitoring 4 temperature measurement points for the interferometer and 2 for the baseplate shown in Figure 1(b). The dates are selected when the temperatures are stable in orbit.

The thermal model is obtained using UG/TMG, UG is a software of Simens for computer-aided design, analysis, and manufacturing, widely used in modern engineering applications, and TMG is a specialized thermal analysis module that can simulate and calculate orbital heat transfer in space environments. The mesh diagram shown as Figure 1(c).

To verify the effectiveness of the correlation method, it is essential to select an initial operating condition, which is named test case. To further assess the generalizability of the correlated thermal model for the project, an additional verification must be conducted under a different operating condition named validation case. Therefore, both test and validation cases are required. Then, the cold case is selected as the test case, and the hot case is selected as the validation case. The boundary conditions for the two operating cases are as follows in the Table 2 below.

The optical payload has three operating conditions: 10 °C, 15 °C, and 20 °C. As the temperature difference between the two operating conditions increases, the demand for the generalization capability of the correlated thermal model also rises, enhancing the credibility of the verification results. Therefore, to more clearly demonstrate that the correlated model remains well-suited under different conditions, we chose the two conditions with the largest temperature difference: 10 °C and 20 °C. All the optical and electrical instruments are controlled of 10 ℃ in cold case or 20 ℃ in hot case except the laser and laser controller.

To maintain its temperature level in 10 ℃ or 20 ℃, thermal control measures, including insulation, heating, and heat dissipation, are necessary for the load. The specific measures implemented are summarized in Table 3. These measures, in conjunction with Figure 1(a) and Figure 1(b), clearly show the location of each thermal control action, the type and quantity of thermal control

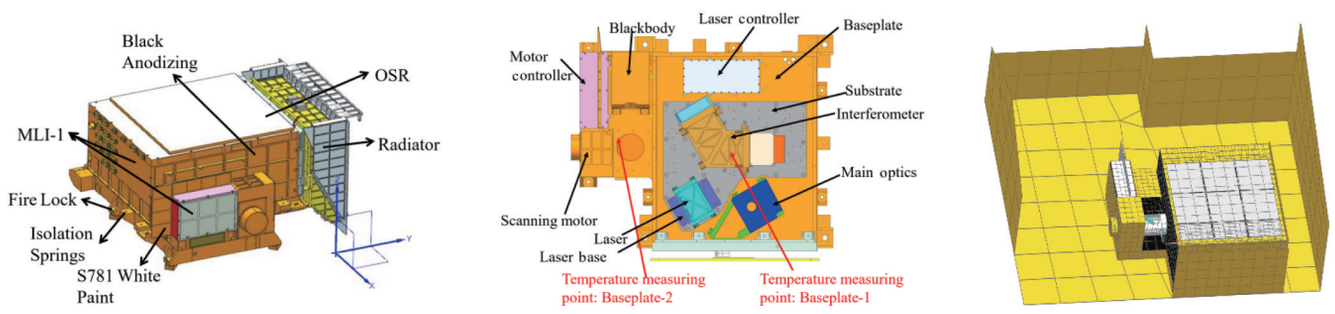

Fig. 1 Model of FY-3E/HIRAS-II: (a) physical model and thermal control measures; (b) distribution of internal components and measuring point of baseplate; (c) mesh of the thermal model for FY-3E/HIRAS-II

图 1 FY-3E/HIRAS-II模型:(a) 物理模型与热控措施; (b) 内部部件结构与底板测温点; (c) FY-3E/HIRAS-II热模型网格

Table 2 The boundary conditions for the two cases

表 2 两种工况的边界条件

Case	Optics temperature	Date	Satellite platform temperature	Laser temperature	Radiator temperature
Cold	10 ℃	2021.10.16	0 ℃	35 ℃	−63 ℃
Hot	20 ℃	2022.9.16	30 ℃	45 ℃	−50 ℃

components used, their installation methods, and the final effects achieved through these measures.

1.2 Parameters

UG/TMG uses a conservative, element-based control volume formulation to compute accurate conductive and capacitive terms for arbitrary, unstructured meshes. The proprietary scheme is based on an element temperature function constrained at calculation points on the boundaries and at the geometric centroid. The resulting solution matrix is extremely accurate, stable and fully compatible with finite difference solvers. Usually, when the optical payload components reach thermal equilibrium in space, their every calculation point should have a thermal equilibrium relationship like Eq. (1). The thermal control equation for this node is mainly a constant temperature boundary condition, as shown in Table 2.

$$\sum_{j}^{s} D_{ji}(T_j - T_i) + \sum_{j}^{w} R_{ji}\sigma(T_j^4 - T_i^4) + Q_i = C_i\frac{\mathrm{d}T_i}{\mathrm{d}\tau}, \quad (1)$$

where j is the point adjacent to point i, T_i and T_j denote their temperature. There are s nodes that have a thermal conductivity relationship with this point, and w nodes that have a radiation relationship with it. D_{ji} is the coefficient of the conduction between points, R_{ji} is the coefficient of radiation between points, Q_i is the total heat source of the point. And the material heat capacity is C_i.

D_{ji} includes contact thermal resistance r, material thermal conductivity h. R_{ji} includes solar absorption rate α_s and hemispherical emissivity ε_H. The total Q_i is composed of the heat source q_i generated by several components.

Therefore, for steady-state problems, the parameters that determine the temperature level of space optical payloads mainly include as follows: r, h, α_s, ε_H, and q_i. To make the thermal model more accurate, these parameters are the parameters to be correlated. Based on the above figures and thermal control methods in Table 3, the parameters to be correlated can be classified into three categories: radiation parameters, corresponding to α_s and ε_H; thermal conduction parameters, corresponding to r and h; and heat consumption parameters, corresponding to q. For the subsequent model correlation, an experimental design is required to generate multiple data sets. Therefore, it is essential to define the value range for each parameter in advance, the main parameters and their value ranges are listed in Table 4, Table 5 and Table 6.

It should be noted that although the initial values for other dry contacts are uniform in Table 5, the dry contact heat transfer coefficients between each component may have some slight deviations due to different processing techniques such as the uncertainty of clamping force, surface treatment process and so on. Thus, they should be handled separately during the process of correlation.

Otherwise, there are 2 kinds of heat sources: one is produced by the components in Table 6, the other one is from the heaters controlled by PID or inherent to the instruments. The former should be correlated because it is unknown exactly, while the latter can be simply calculated like Table 7 based on the duty cycle in orbit.

There are a total of 44 input parameters to be corrected, including 11 for radiation, 29 for thermal conduction, and 4 for heating consumption. And the output parameters include a total of 6 temperature values for interferometer 1-4, baseplate 1-2.

2 Method of correlation

The structure of Intelligent Correlation Platform for

Table 3 Measures to control temperature
表 3 控温措施

Measures	Method	Position	Purpose
Surface treatment	OSR (Optical Solar Reflector)	OSR panel	To promptly dissipate excess heat from the interior and make efficient use of the cold space background.
	S781 white paint	$+Z$ and $-Y$ surfaces of the motor controller and the $+X$ side of the fins	
Wrap MLI (Multi-Layer Insulation)	PI (polyimide) second surface mirrors as the outermost layer (named MLI-1)	The surface of shell except $+X$	To mitigate the impact of external heat flux, primarily from solar radiation.
	Carburized black membrane (named MLI-2)	The outer surface of the interferometer, laser, and main optics	
Insulation installation	4 installation feet are connected by TC4 (a kind of titanium alloy) isolation springs, and an 8mm thick insulation gasket of PI. 6 installation feet are connected to the fire lock, and there is a 3mm insulation gasket of PI.	Between the baseplate and satellite	The payload is in contact with two thermal platforms: the satellite platform at normal temperature, and the radiator at a low temperature. In order to minimize their impact on the payload.
Blackening treatment	Black anodizing treatment	The interferometer, scanning motor and the surface of shell	To reduce the influence of stray light.
Thermal homogeneity	High thermal conductivity graphite sheets	The outer surface of the interferometer	To maintain the temperature of the internal lenses of the interferometer at the same level and temperature gradients.

The high thermal conductivity graphite sheets resulting in the temperatures of the four temperature measuring points of the interferometer being very close, therefore, detailed positions are not provided in Fig. 1(b).

Table 4 Parameters to be correlated – thermal radiation
表 4 待标校参数–热辐射类

Material	ε_H			α_S		
	Name	Initial value	Range	Name	Initial value	Range
MLI-1	ε_1	0.65	[0.62,0.72]	α_1	0.35	[0.3,0.55]
MLI-2	ε_2	0.88	[0.8,0.9]	α_2	0.93	[0.9,0.95]
S781 white paint	ε_3	0.87	[0.81,0.93]	α_3	0.17	[0.11,0.4]
OSR	ε_4	0.8	[0.76,0.88]	α_4	0.16	[0.08,0.3]
Black anodizing	ε_5	0.9	[0.88,0.98]	α_5	0.96	[0.86,0.96]
PCB surface	ε_6	0.9	[0.81,0.95]	/	/	/

The PCB surface is completely located inside and not exposed to sunlight, its solar emissivity is not correlated.

Table 5 Parameters to be correlated – thermal conduction
表 5 待标校参数–导热类

Conductive components	Parameters	Name	Initial value	Range
Between laser controller and baseplate	h(W/(m^2·K))	h_1	3000	[2000, 4000]
Between interferometer and substrate		h_2	300	[100,600]
Between parts of interferometer		h_3	500	[300, 1000]
Between MLI and components be warped		h_4	0.05	[0.03, 0.09]
Between laser base and substrate		h_5	100	[50,400]
Between shell and baseplate		h_6	100	[50,400]
Between OSR and roof		h_7	100	[50,400]
Between motor and fin		h_8	100	[50,400]
Other dry contacts		h_9~ h_{21}	100	[50,400]
Between laser and laser base	r (K/W)	r_1	20	[5,50]
Isolation springs		r_2	500	[50,600]
Fire lock		r_3	20	[5,25]
Between shell and radiator		r_4	20	[5,25]

Table 6 Parameters to be correlated – Heat consumption
表 6 待标校参数–热耗类

Heating Components	Name	Initial value /W	Range/W
Motor controller	q_1	12	[10,14]
Laser controller	q_2	14	[12,14]
Data transmission	q_3	1.4	[1,3]
Scanning motor	q_4	4.6	[2,5]

Thermal Model (ICP-TM) is shown as Figure 2, which has achieved automated, intelligent and precise correlation process of thermal model for infrared payloads. It is primarily divided into three modules: a, b, and c, which will be introduced separately below.

Table 7 The actual heating output of the thin heating elements in orbit
表 7 薄膜加热片在轨实际发热量

Component be heated	Actual heating power/W	
	10 ℃ case	20 ℃ case
Baseplate-1	10.49	16.74
Baseplate-2	2.81	3.88
Interferometer -1	0.15	0.31
Interferometer -3	0.05	0.15
Moving mirror	1	1
Data collector	9	9
Front box	15.9	15.9

2.1 Establish a workflow

Establish an automated workflow in optimization software like Optimus, which includes input parameters, running macro files (macro files are recorded by simulation software like UG and mapped between parameter matrices in optimization software like Optimus, then rewrite new macro files to run), simulation calculations, and exporting temperature results. Replace the input parameters with LHS (Latin Hypercube Sampling) in the macro file to do iterative calculations, and repeat it until the iteration reaches N_{min} calculated by the Eq. (2)[14] decided by sensitivity analysis. Determining the initial required sample size for sensitivity analysis can be done using the confidence interval method. The first idea that should be introduced is that "It is important to understand that the output samples from simple Monte Carlo consists of independent output values from the output distribution, irrespective of the number of uncertain inputs"[15]. A commonly used approach is to calculate the width of the confidence interval for parameter estimation and then determine the sample size based on the desired confidence level and precision.

$$N_{min} = \left(\frac{2N_\sigma s}{\Delta x}\right)^2 \quad , \quad (2)$$

where Δx is the width of the interval in which the mean is expected to be found with a confidence level given by N_σ. When the confidence level is 95%, then N_σ =1.96. For this question, an accuracy of ±0.2 ℃ (Δx =0.4 ℃) is sufficient. If the initial estimate of the standard deviation for a node temperature is s =2 ℃, a Monte Carlo simulation with N_{min}=384 runs of the model will assure.

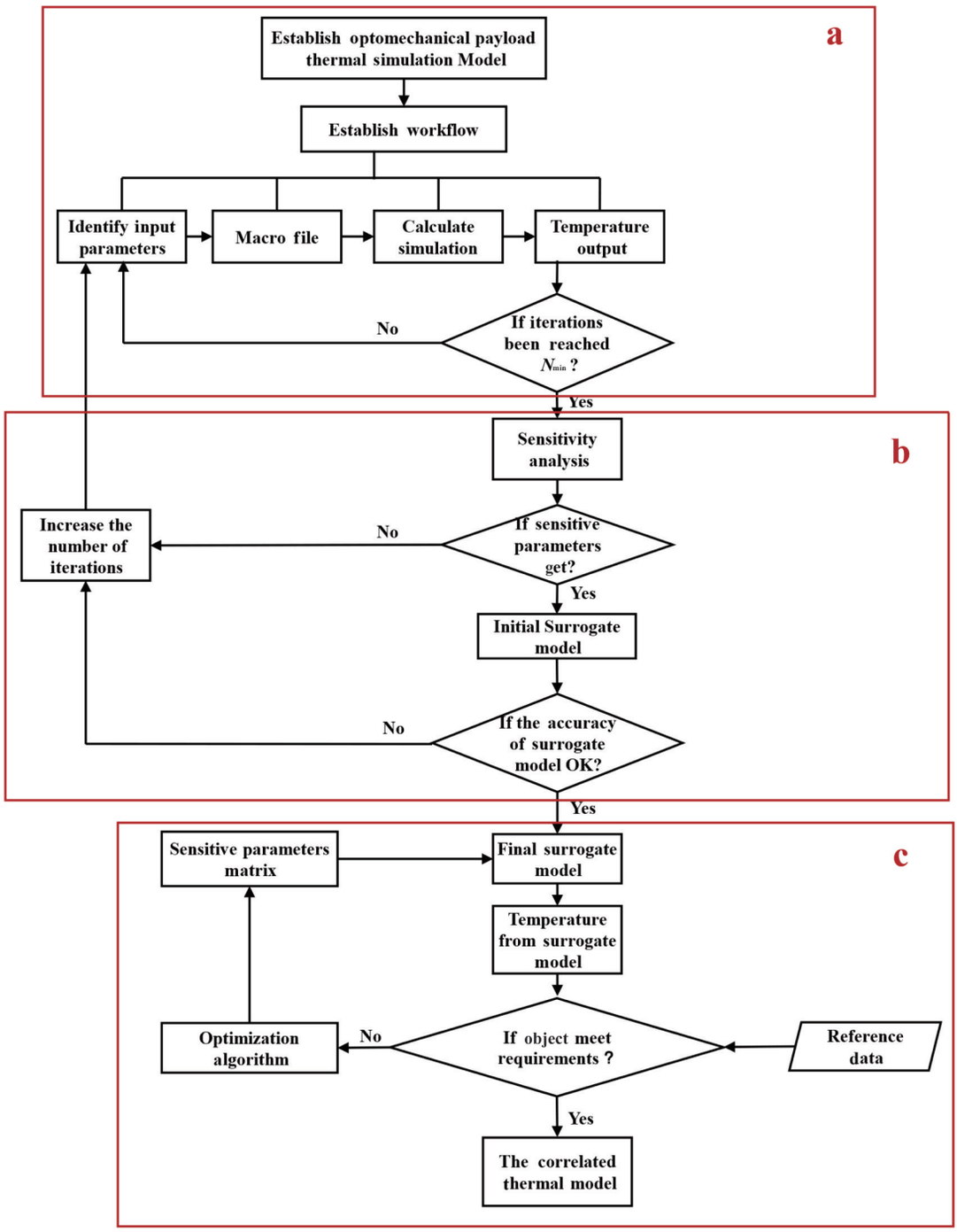

Fig. 2 Flowchart of ICP-TM
图 2 ICP-TM工作流

2.2 Sensitivity analysis and build surrogate model

To reduce the dimensional of the problem and identify the input parameters that have the greatest impact on the temperature results of the optical payload, it is necessary to conduct sensitivity analysis in a targeted and directional manner by correlating them with reference data [16]. The sensitivity parameters are used as input parameters, and the calculated temperature is used as output parameters to construct a surrogate model. The Spearman rank coefficient was widely used to rank the degree of influence of input variables on output [17]. The coefficient is calculated by the Eq. (3)[18].

$$R_S = 1 - \frac{6\sum_{i=1}^{m}[P(C_i) - P(T_i)]^2}{m(m^2 - 1)} \quad , \quad (3)$$

where m is the sample size of training, C_i represents the temperature calculated by simulation, T_i represents the temperature predicted by the surrogate model. The larger the R_S value, the greater the impact of this parameter on temperature results.

Once the sensitivity parameters are obtained, the input parameters are significantly simplified, thereby establishing a mapping relationship between the sensitivity parameters and the output temperature results, and this relationship can be called surrogate model. Such a surrogate model can replace simulation calculations, thereby improving the efficiency of subsequent parameter optimization. Many standard machine learning models have emerged to replace simulation methods with surrogate models[19, 20], like Kriging (Or Gaussian process)[21], ANN[22] (Artificial Neural Network), DNN[23, 24] (Deep Neural Network), RBF[25] (Radial Basis Function) or SVR[26] (Support Vector Regression) and so on. All of these models have been used for surrogate models instead of simulation, among them Kriging is particularly suitable for replacing computer simulation models and has strengths shown as following[27, 28].

(1) Appropriate for highly nonlinear problems;

(2) Well-suited for data with deterministic errors;

(3) Suitable for applying to problems up to 50 parameters;

(4) More accurate approximations over a wide range of sample size.

The Kriging model, an optimal linear unbiased estimation method, was initially used in geological research and then gradually applied in aerospace, automotive, materials processing, etc. [29] Recently, due to its efficiency and accuracy, Kriging interpolation has been one of the most favored methods in the aerospace applications[28-31]. It uses a simple linear regression to outline the shape of the interpolated surface after training points, and incorporates a random process to approximate the response surface of real data by weighting the correlation of nearby points[32]. It can be described as the Eq. (4)[30].

$$\hat{f}_{\mathrm{kri}}(\boldsymbol{X}) = F(\boldsymbol{\beta},\boldsymbol{x}) + \varepsilon(\boldsymbol{x}) = \boldsymbol{f}^{\mathrm{T}}(\boldsymbol{x})\boldsymbol{\beta} + \varepsilon(\boldsymbol{x}) \quad , \quad (4)$$

where $\boldsymbol{f}^{T}(\boldsymbol{x})$ is a polynomial vector of the training sample$\boldsymbol{x}$, the term approximates the drift; $\boldsymbol{\beta}$ is regression parameters, they are obtained through Maximum Likelihood Estimation (MLE), which makes them most consistent with the observed data. The method relies on the assumption that the observed data is the result of a Gaussian process; $\varepsilon(\boldsymbol{x})$ is the realization of the stochastic process approximates the local deviation; $\boldsymbol{X}$ including $\boldsymbol{X}_i, \boldsymbol{X}_j$ are two training samples. According to the thermal analysis in section 2.1, for this issue, the input parameters of the surrogate model include α_{S}, ε_{H}, h, R, R_1, and Q mainly. Define sampling points as $\boldsymbol{x} = \{x_1, x_2, \cdots, x_n\} \subset \Re^n$, where x is the value of the input parameter, $\Re^n$ is n-dimensional Euclidean space, i. e. parameter space, which determines the range of parameter values. Then, the input spatial sampling point matrix is $\boldsymbol{X} = [\boldsymbol{X}_1, \boldsymbol{X}_2, \cdots, \boldsymbol{X}_N]^{\mathrm{T}}$. The output parameters are temperature of key points of components mainly. Similarly, a single temperature output is defined as $\boldsymbol{t} = \{T_1, T_2, \cdots, T_m\}$, where T is the output parameter temperature. The output spatial sampling point temperature matrix is $\boldsymbol{T} = [\boldsymbol{t}_1, \boldsymbol{t}_2, \cdots, \boldsymbol{t}_N]^{\mathrm{T}}$. The detailed calculation principles regarding this formula can be found in reference [33].

The size of co-ownership N sampling points of the data sets are generally determined by the Eq. (5)[34].

$$N = \frac{n(n+1)}{2} \quad , \quad (5)$$

where n represents the number of input parameters x. If the number of iterations for sensitivity analysis in Eq. (2) is less than N, further increasing the number of simulation runs is necessary to ensure the accuracy of the surrogate model.

To meet the accuracy requirements of surrogate model, we need to take into account the accuracy and time-cost simultaneously. The most commonly used method in reality is to use the expected test error on the test set to calculate generalization error. Therefore, we often divided the data sets into 80 % training set, 10 % validation set, and 10 % test set. After the model training is completed, the training error and validation error of the surrogate model can generally be represented by MSE (Mean Square Error) for test set, which is the average square of the overall prediction error on the test data sets based on Eq. (6)[25].

$$\mathrm{MSE} = \frac{1}{N_{\mathrm{test}}} \sum_{i=1}^{N_{\mathrm{test}}} (y_i - \hat{y}_i)^2 \quad , \quad (6)$$

where N_{test} is the sample size, y_i represents the calculated temperature value of simulation, $\hat{y}_i$ represents the temperature prediction value of the surrogate model. The smaller the MSE, the better the quality of the surrogate model.

2.3 Optimization

The criterion for determining the correlation effect is achieved using a function. The Object refers to a function that represents the deviation between the experimental temperature data E_i and the calculated temperature data C_i, as shown in Eq. (7).

$$\mathrm{Object} = \min\left(\sum_{i=1}^{N} (C_i - E_i)^2\right) \quad . \quad (7)$$

Due to the adaptive optimization algorithm finds the optimal point by gradually reducing the area of interest around the point, it can gradually improve and optimize the model with the increase in data and experience, achieving better results and accuracy. Therefore, in the subsequent parameter optimization, the adaptive optimization algorithm is used to optimize the parameters. The implementation steps[35] of this algorithm are shown as following Figure 3.

Where y_k^{Kriging} is the value of the output variable calculated by the Kriging surrogate model in iteration.

Through the above process, the input parameters are iterative optimized based on the Kriging surrogate model. After determining the main correlation methods for the ICP-TM platform, the thermal model for infrared payloads on FY-3E/HIRAS-II can be correlated to in-orbit data.

3 Results and discussion

3.1 Sensitivity analysis

According to Eq. (2), a total of 384 simulations have been calculated after iterative calculation of simulation and calculating this Spearman rank correlation coeffi-

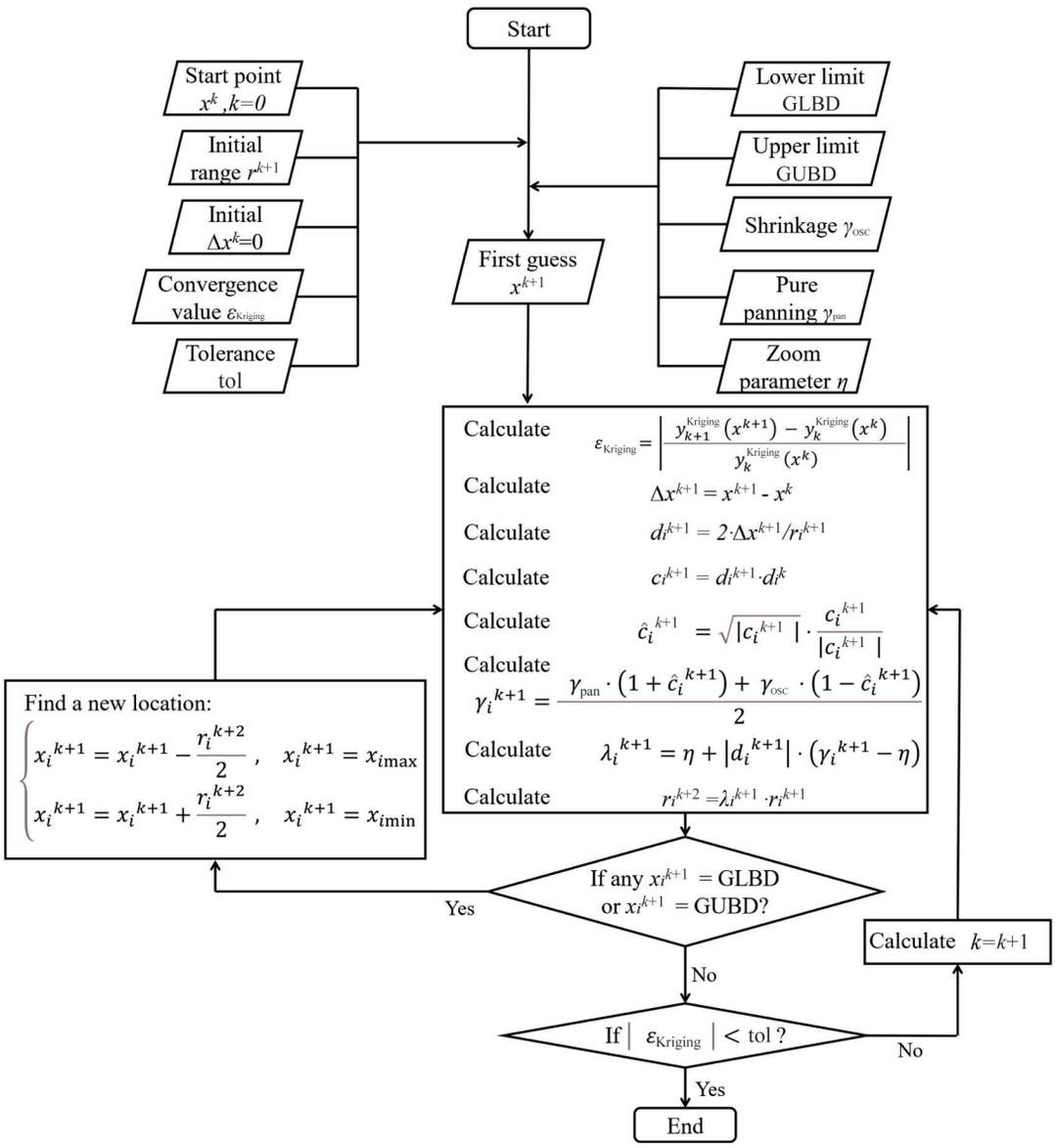

Fig. 3 Flowchart of adaptive region algorithms
图 3 自适应区域算法流程图

cient by ICP-TM. Finally, the sampling characteristics of input parameters follow uniform distributions, the mean and variance of the output temperature results tend to stabilize. The sensitivity parameters obtained from each sensitivity analysis tend to stabilize to a total of 13 sensitive parameters. Thus, the sample set is sufficient to reflect the sensitivity situation.

Due to the placement of uniform temperature graphite sheets on the surface of the interferometer, the temperature differences among the four temperature measuring points are very small. Consequently, the obtained sensitivity parameters are also very close as shown as Fig. 4(a). However, for the two measuring points on the baseplate, as shown in Fig. 1(b), one is located at the bottom of the optical component baseplate and the other at the bottom of the motor component baseplate. Therefore, their sensitivity parameters need to be considered separately shown as Fig. 4(b) and Fig. 4(c).

According to Fig. 4(a),(b),(c), in the 44 parameters, there are totals of 13 input parameters, all of which have significant impacts on the readings of the three temperature measuring points. The sensitive parameters of the interferometer and the baseplate-1 are very similar because their positions are close. The parameters that have the greatest influence ($1>R_s\geqslant 0.3$) on their temperatures are the contact resistance between the shell and radiator (r_4), fire lock (r_3), between the laser and laser base (r_1). This indicates that the overall temperature level of the payload primarily depends on the temperature boundary conditions with surrounding components, which is consistent with our general understanding. The parameters that have the general influence ($0.3>R_s\geqslant 0.2$) on their temperatures are the thermal conductivity directly related to heat or cold sources heat flux boundary con-

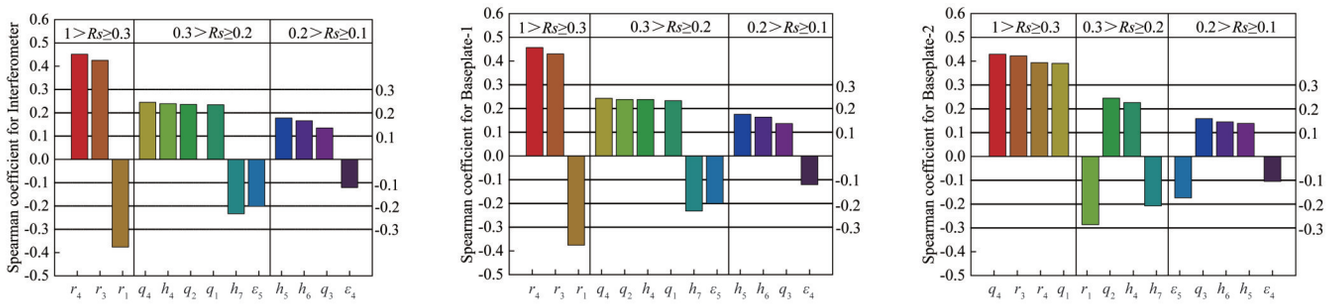

Fig. 4 Spearman coefficient of parameters:(a) interferometer ;(b) baseplate-1; (c) baseplate-2
图 4 参数的斯皮尔曼相关性系数:(a)干涉仪 ;(b) 底板-1 ;(c)底板-2

ditions, like q_4, q_2, q_1, h_4, h_7, and the infrared emissivity of black anodizing. The heat transfer coefficient h_5 and h_6, heat consumption q_3 and the emissivity of OSR (ε_4) have slight influence($0.2>R_s\geqslant 0.1$), and the other 31 parameters are not sensitive.

The temperature measuring point of the baseplate-2 is located near the scanning motor, motor controller, and black body, hence it will also be influenced by the temperature levels of these components. Of course, it will also be influenced by the temperature boundary conditions of the surrounding environment. Thus, the greatest sensitive parameters are the heat from scanning motor (q_4) and motor controller (q_1). The differences of other parameters with the previous ones are not significant.

Specifically, some parameters have positive sensitivity coefficients, while others have negative ones. This indicates whether the parameters are positively or negatively correlated with temperature. Overall, an increase in parameters related to heat sources tends to raise the load temperature like q_1, q_2, q_3, q_4. When there is increased heat transfer at the high-temperature boundary, the load temperature rises like r_1, h_5. Conversely, when there is increased thermal resistance at the low-temperature boundary, the load temperature also rises like, r_4, r_3, h_7. The higher the emissivity of the heat dissipation surface, the stronger the heat dissipation ability, resulting in lower temperatures like ε_4 and ε_5. When the contact between the shell and the baseplate is better, the temperature uniformity of the load improves. Higher shell temperatures reduce the heat dissipation of internal loads, therefore h_6 is negatively correlated with temperature.

3.2 Correlation

Take the 13 sensitive input parameters and 6 output temperature parameters into building the Kriging surrogate model by ICP-TM. The statistical results of the surrogate model are shown in Table 8 and Table 9.

According to Eq. (5), for the 13 input parameters, at least 91 iterations of simulated data sets are required. The data set used in the previous sensitivity analysis was quite sufficient, so there is no need to increase the data set further. Firstly, in terms of the time-cost, it is indicated that after using the Kriging surrogate model, the time of simulation can be shortened from 1 h 25 min to less than 0.1 s, the computational efficiency has been greatly improved, which is extremely beneficial for subsequent parameter optimization. Secondly, in terms of the accuracy of surrogate model, for test data set, the average predicted temperature error is within 0.4 K. In summary, for the demands for high-dimensional input parameters, strong non-linearity, high accuracy and computational efficiency of thermal model for space borne optical payloads, the Kriging surrogate model can meet all of them currently, especially for this case.

Table 8 Results of surrogate model
表 8 代理模型结果

Evaluating indicator	Result
Time for training	33 min53 s
Time for single calculate	less than 0.1 s
MSE of test data set	0.188
Average absolute prediction error	0.369 K

After establishing the surrogate model, it is turned to perform optimization on the ICP-TM platform with Object based on Eq. (7). The settings for the adaptive region algorithm are: Population size-240; Average termination step-0.01; Maximum iteration count-300, From this, up to 72,000 computation points can be generated. Actually, the Object has already converged after only 43 iterations with 10,560 computations, the optimization process took only about 1 minute. The comparison of the total time cost between ICP-TM and manual correlation is shown in Table 9.

Table 9 Time-cost compared between ICP-TM and manual correlation
表 9 ICP-TM与手动标校的耗时对比

Method	Process	Time-cost of single process	Total time-cost
Manual	Manual correlation	About 3 months	About 3 months
ICP-TM	Iterative simulation of 384 data set	About 7 days with 3 computers	In 8 days
	Build Kriging surrogate model	In 34 min	
	Adaptive optimization	In 1 min	

Both manual and ICP-TM correlations were performed on an HP (Hewlett-Packard, a computer brand) Z840 desktop workstation equipped with a 32-core processor. The UG software used was the 2015 version, and all TMG simulation calculations were executed using a 10-core parallel processing configuration. As both calibration methods were conducted under identical hardware conditions, this setup allows for a direct comparison of computational efficiency.

In general manual correlation, the correlation works heavily relies on the engineer's experience and familiarity with the project. As a result, it is usually performed by a single engineer on a single computer. Furthermore, it is possible to make mistakes during each time the thermal model parameters are modified. Even for a senior engineer, 3 months is still quite tight. However, as for ICP-TM, firstly, it avoids the issue of making coarse mistakes when changing parameters by automated sampling and playback macro file. Secondly, compared to manual correlation, ICP-TM has reduced time costs by more than two-thirds overall. Although it is undeniable that the most time-consuming process is iterative simulation and construction of data set, it runs automatically once established, the time cost can be reduced by parallel computing on computers and merging data sets. The time cost has been reduced from 3 months to 8 days, approximately a 90% decrease.

After substituting the optimal parameters back into the simulation model, the temperature cloud map of cold case is shown as Figure 5(a). By comparing the temperature in orbit, predicted by surrogate model, calculated by correlated simulation model, and calculated by pre-correlated simulation model together, we can quantitatively evaluate the effectiveness and performance of the ICP-TM platform. The comparison is shown in Figure 5 (b) and Figure 5(c). It is important to note that in Figure 5(b), due to the calibration accuracy of the thermistor being 0.5 K, there will be ±0.5 K errors in temperature measurements in orbit. To more clearly observe whether the associated errors fall within ±1 K, we have additionally included curves for +1 K and -1 K. Errors beyond this range are considered to be outside the ±1 K accuracy threshold.

The result indicates that the error of predication for main temperature control components have reached within ± 1 K from 5 K with the in-orbit temperature after the correlation. This result is more optimistic than the results found like 3 K in current literature in Table 1. We have met the accuracy requirements of the payload in cold case for thermal model correlation.

Furthermore, whether the optimal parameters obtained under cold conditions are applicable to other operating conditions of the model needs further validation.

3.3 Validation

Based on Table 2, we selected the hot case for further validation. To ensure that the results are solely related to changes in operating conditions, none other changes were made to the model structure and settings. After calculation, the temperature cloud map of hot case is shown as Figure 6(a). We compared the temperature of simulation after the correlation with the original simulation and in-orbit temperature. This indicates that these temperature sensors can roughly characterize the applicability of the optimal parameter combination obtained from correlation to the hot case. The results are shown in Figure 6(b) and Figure 6(c).

It is indicated that most of these 6 measurement points meet the expected prediction error within ±1 K except for the sensors on the baseplate-2, approximately 1.4 K lower than in-orbit data. More detail, after the correlation, the temperatures were slightly lower than the in-orbit temperatures for most measurement points in cold case, while in hot case, they were mostly higher. Specifically, the temperature of baseplate-2 is not necessarily the case. For these 2 special phenomena, they may be because of the 4 reasons:

(1) Due to the degradation of some coatings, affected by the space environment resulting in a slight change in payload heat dissipation capacity, like the increasing of solar absorption rate of OSR, result in the rising of temperature.

(2) Due to the temperature difference between the two cases, different temperatures may cause changes in the thermal physical properties of the parameters.

(3) Due to different temperature boundaries, the model may experience errors. The results of correlation only obtained sensitive parameters, which cannot reflect the complete physical model.

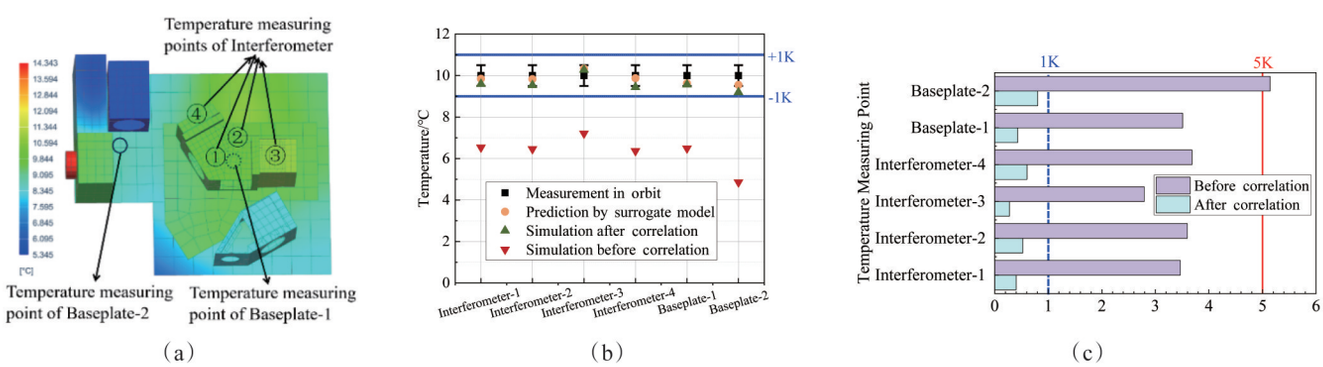

(a) (b) (c)

Fig 5 Correlation result of cold case for FY-3E/HIRAS-II:: (a) temperature cloud map ; (b) correlation results of temperature comparison ; (c) absolute error

图 5 低温工况下FY-3E/HIRAS-II的标校结果:(a) 温度云图;(b)温度标校结果对比 ;(c) 绝对误差

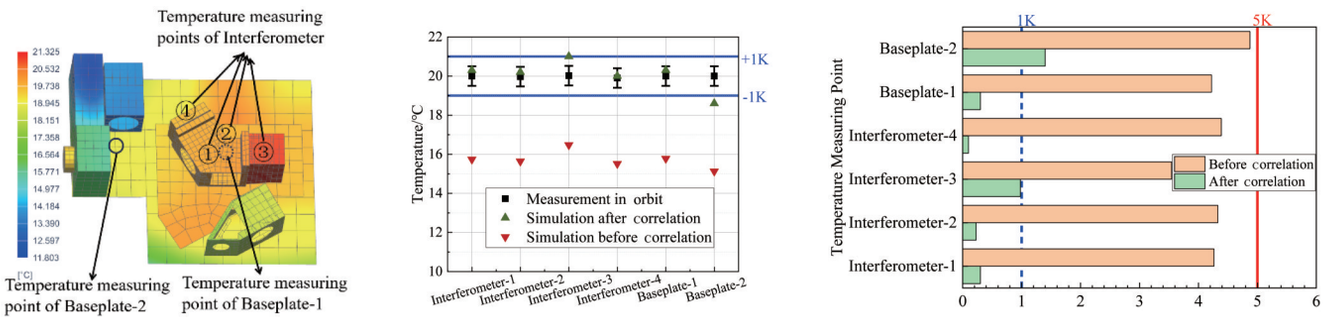

(a) (b) (c)

Fig. 6 Correlation result of hot case for FY-3E/HIRAS-II: (a) temperature cloud map; (b) correlation results of temperature comparison ; (c)Absolute error

图 6 高温工况下FY-3E/HIRAS-II的标校结果:(a) 温度云图 ;(b)温度标校结果对比; (c) 绝对误差

(4) Due to the location of the sensor of baseplate-2, it is closer to exposed areas than others. Perhaps it receives greater interference from changes in external heat flux.

Although not all points have errors within ±1 K like the cold case, this result is still inspired that represents a significant improvement compared to the overall prediction error of approximately 5 K before the correlation or 3 K in other literature.

3.4 Discussion

The proposed approach does have limitations. To further define the scope and conditions for applying the method discussed in this paper, the following recommendations based on its inherent characteristics are offered:

(1) Due to the "black box" nature of the DNN surrogate model used in the calibration process, there is a partial disconnect from the underlying thermal processes. As a result, the thermal parameters obtained through ICP-TM may not represent true physical values. Therefore, it is essential to use the calibrated thermal model and its thermal parameters together as a set.

(2) The logic and approach of the ICP-TM method are theoretically universal in the field of thermal model correlation, because the process involves generally parameter identification, surrogate model construction, and parameter optimization. However, thermal models can vary significantly across different projects, and even across different operating conditions within the same project. Thus, the generalization capability of the correlated thermal model must be robust.

(3) The establishment of the surrogate models in this method is based on data sets generated from hundreds of iterations of experimental design using the original thermal model. If the physical model or basic structure of the original model changes, the previously generated data set will largely lose its relevance, necessitating new iterations to generate a fresh data set—thereby exponentially increasing time costs. Therefore, it is advisable to employ this method only after the project's physical model and the thermal boundaries with surrounding components are firmly established.

In future research, to ensure the correlation results are equally applicable in validation cases or other operating cases, considerations can be made in the following 2 aspects:

(1) Further refinement is needed in improving the prediction accuracy of the Kriging surrogate model through improved algorithms to meet the requirements for higher precision in projects such as black body calibration components.

(2) The current parameters, being the results of optimization, may to some extent lose their physical significance and may not represent the true values. Subsequent correlation results from multiple projects could potentially derive more universally applicable parameters or patterns of parameter values through big data analysis.

4 Summary

A study on method named ICP-TM was established in this paper by building convenient workflow, sensitivity analysis, constructing advanced Kriging surrogate model, and using efficient adaptive region optimization algorithm. It achieved an intelligent and automated process for correlating the thermal model with in-orbit data for infrared optical payloads on FY-3E/HIRAS-II.

It has been verified of the feasibility and superiority of this platform in cold and hot cases. It greatly improves the efficiency of thermal model correlation about 90% from 3 months to 8 days, and the accuracy of thermal model prediction has been improved significantly within ±1 K compared with 5 K before the correlation or 3 K in other literature. This work is of great significance for precise thermal design and temperature prediction for infrared payloads in orbit.

References

[1] Toussaint M. Verification of the thermal mathematical model for artificial satellites – a new test philosophy [C] AIAA. proceedings of the 2nd Thermophysics Specialist Conference. AIAA, 1967.

[2] Ishimoto T, Gaski J D, Fink L C. Development of digital computer program for thermal network correction: NASA-CR-108681 [R]. NASA, 1970.

[3] Shimoji S. A comparison of thermal network correction methods [C] AIAA. proceedings of the 16th Thermophysics Conference. New York, NY, USA: AIAA, 1981.

[4] Boisvert P, Rheault S, Theophanous P, et al. Verification of Envisat ASAR active antenna thermal design by a thorough sensitivity analysis[J]. JOURNAL OF AEROSPACE, 1997, 1101-1109.

[5] Herrera F L, Sepulveda A T. Stochastic approach to spacecraft thermal control subsystem[C]ICES. proceedings of the International Conference on Environmental Systems. 2000.
[6] Beck T, Bieler A, Thomas N. Numerical thermal mathematical model correlation to thermal balance test using adaptive particle swarm optimization (APSO) [J]. Applied Thermal Engineering, 2012: 168-174.
[7] Anglada E, Martinez-Jimenez L, Garmendia I. Performance of gradient-based solutions versus genetic algorithms in the correlation of thermal mathematical models of spacecrafts[J]. International Journal of Aerospace Engineering, 2017, 2017: 1-12.
[8] Anglada E, Garmendia I. Correlation of thermal mathematical models for thermal control of space vehicles by means of genetic algorithms[J]. Acta Astronautica, 2015, 108: 1-17.
[9] Kim J S, Kim H D. Thermal model correlation and validation of a 6U nanosatellite with multiple payloads [J]. International Journal of Aeronautical and Space Sciences, 2022, 23(1): 207-220.
[10] Shin S, Lim J H, Kim C-G. Thermal parameter determination in underdetermined spacecraft thermal models using surrogate modeling [J]. Acta Astronautica, 2024, 214: 583-592.
[11] Li W, Xiao M, Peng X, et al. A surrogate thermal modeling and parametric optimization of battery pack with air cooling for EVs[J]. Applied Thermal Engineering, 2019, 147: 90-100.
[12] Cui Q, Lin G, Cao D, et al. Thermal design parameters analysis and model updating using Kriging model for space instruments[J]. International Journal of Thermal Sciences, 2022, 171.
[13] Zhang P, Xiuqing H U, Qifeng L U, et al. FY-3E: The first operational meteorological satellite mission in an early morning orbit[J]. Advances in Atmospheric Sciences, 2022, 39(1): 1-8.
[14] Gómez-San-Juan A, Pérez-Grande I, Sanz-Andrés A. Uncertainty calculation for spacecraft thermal models using a generalized SEA method[J]. Acta Astronautica, 2018, 151: 691-702.
[15] Morgan. M G, Henrion. M. Uncertainty: A Guide to Dealing with Uncertainty in Quantitative Risk and Policy Analysis[M]. 1996.
[16] Pohya A A, Kai W, Kilian T. Introducing variance-based global sensitivity analysis for uncertainty enabled operational and economic aircraft technology assessment[J]. Aerospace Science and Technology, 2022, 122: 107441.
[17] Allard A, Fischer N. Recommended Tools for Sensitivity Analysis Associated to the Evaluation of Measurement Uncertainty[M]. Advanced Mathematical And Computational Tools In Metrology And Testing IX, 2015.
[18] Dodge Y. Spearman Rank Correlation Coefficient[M]. Springer New York, 2006.
[19] Gogu C, Haftka R T, Bapanapalli S K, et al. Dimensionality reduction approach for response surface approximations: application to thermal design[J]. AIAA Journal, 2009, 47(7): 1700-1708.
[20] Jin R, CHEN W, Simpson T M. Comparative studies of metamodeling techniques under multiple modeling criteria[J]. Structural and Multidisciplinary Optimization, 2001, 23.
[21] Xu H, Li H, Xiang G, et al. An improved adaptive surrogate model and application in thermal management system design[J]. Materials & Design, 2021, 208: 109883.
[22] Klement J. On using quasi-newton algorithms of the broyden class for model-to-test correlation [J]. J Aerosp Technol. Manag, 2014, 6 (4): 407-414.
[23] Xiong Y, Guo L, Zhang Y, et al. Surrogate modeling for spacecraft thermophysical models using deep learning[J]. Neural Computing and Applications, 2022, 34(19): 16577-16603.
[24] Tao J, Sun G. Application of deep learning based multi-fidelity surrogate model to robust aerodynamic design optimization [J]. Aerospace Science and Technology, 2019, 92: 722-737.
[25] Jiang P, Zhou Q, Shao X. Surrogate model-based engineering design and optimization[M]. 2020.
[26] Zhao D, Liu D, Zhu M. A surrogate model for thermal characteristics of stratospheric airship[J]. Advances in Space Research, 2018, 61 (12): 2989-3001.
[27] Simpson T W , Mauery T M , Korte J J , et al. Comparison of Response Surface and Kriging Models for Multidisciplinary Design Optimization [C]//7th AIAA/USAF/NASA/ISSMO Symposium on Multidisciplinary Analysis and Optimization, 1998. American Institute of Aeronautics and Astronautics, 1998.DOI:10.2514/6.1998-4755.
[28] Mohammadi-Amin M, Entezari M M, Alikhani A. An efficient surrogate-based framework for aerodynamic database development of manned reentry vehicles[J]. Advances in Space Research, 2018, 62 (5): 997-1014.
[29] Zheng C, Zhao H, Zhou Z, et al. Investigation on thermal model updating of Alpha Magnetic Spectrometer in orbit based on Kriging meta-modeling[J]. Nuclear Instruments and Methods in Physics Research Section A: Accelerators, Spectrometers, Detectors and Associated Equipment, 2022, 1031: 166581-.
[30] Ollar J, Mortished C, Jones R, et al. Gradient based hyper-parameter optimisation for well conditioned kriging metamodels[J]. Structural and Multidisciplinary Optimization, 2016, 55(6): 2029-2044.
[31] WANG J T, WANG C J, ZHAO J P. Frequency response function-based model updating using Kriging model[J]. Mechanical Systems and Signal Processing, 2017, 87: 218-228.
[32] Martin J D, Simpson T W. Use of Kriging Models to Approximate Deterministic Computer Models [J]. AIAA Journal, 2004, 43 (4): 853-863.
[33] Wang J, Wang C, Zhao J. Frequency response function-based model updating using Kriging model [J]. Mechanical Systems and Signal Processing, 2017, 87: 218-228.
[34] Garmendia I, Anglada E. Thermal parameters identification in the correlation of spacecraft thermal models against thermal test results [J]. Acta Astronautica, 2022, 191: 270-278.
[35] Gustafsson E, Strömberg N. Optimization of castings by using successive response surface methodology [J]. Structural and Multidisciplinary Optimization, 2006.